Microphase Separation upon Heating in Diblock Copolymer Melts

Junhan Cho[†]

Department of Polymer Science and Engineering, Dankook University, San-8, Hannam-dong, Yongsan-gu, Seoul 140-714, Korea

Received April 12, 2000; Revised Manuscript Received August 10, 2000

ABSTRACT: A mean-field Landau free energy is formulated for a compressible diblock copolymer melt that microphase separates upon heating. Finite compressibility, which induces microphase separation in such a copolymer, is incorporated into the free energy through interaction fields for describing effective interactions between constituent polymers. The condition of microphase separation transition and equilibrium microphase morphologies are determined for the diblock copolymer of deuterated polystyrene and poly(vinyl methyl ether) as a model system exhibiting the thermally induced microphase separation. The Landau analysis reveals that microphase separation transition for the given copolymer is of first order in the entire region of composition. The phase diagram for the copolymer including classical microphase morphologies is shown to be apparently different from that for typical diblock copolymers exhibiting microphase separation upon cooling. In addition, the fluctuations of free volume are analyzed after microphase separation. Excess free volume is shown to be present in the domains of a more compressible component.

I. Introduction

Block copolymers, which are obtained from chemically binding two or more different homopolymers, have drawn enormous interest from polymer engineers because of their nanoscale self-assembly behavior. Various microscopically ordered structures, called microphases, result from such self-association. Block copolymers are, therefore, widely used in a variety of applications as thermoplastic elastomers, compatibilizers, surface modifiers, and photoresists.[1−3]

Block copolymers of incompatible pairs show a microphase separation from a disordered state to an ordered state when system temperature is cooled, which is called the upper critical ordering transition (UCOT) behavior. The origin of UCOT behavior is the unfavorable interactions between polymers comprising a given block copolymer, so that it is analogous to the upper critical solution temperature (UCST) behavior in the corresponding polymer blends. Several ordered morphologies are formed after microphase separation.[1−3] Among them, body-centered-cubic spheres (BCC), hexagonally packed cylinders (HEX), and lamellar (LAM) structures are called classical morphologies. For such morphologies, disorder−order and order−order transitions near stability limits have well been analyzed by using Leibler's incompressible random-phase approximation (RPA) theory.[4] There exist other microphases such as bicontinuous gyroid and hexagonally perforated lamellar structures, which are categorized as complex morphologies. To analyze these complex morphologies, one requires more sophisticated theories with harmonic corrections allowed, suggested by Olvera de la Cruz et al.,[5,6] by Milner and Olmsted,[7] and by Hamley and coworkers.[8−11]

Leibler's RPA theory follows a Landau mean-field approach to phase transitions, in which the free energy is expanded as a series in order parameters.[4] The order parameters are typically given by density or concentration fluctuations in a given system. From the analysis of the formulated Landau free energy of quartic order, it was shown by Leibler that a typical UCOT diblock copolymer exhibits a first-order transition from a disordered state to a BCC morphology upon cooling with the exception of a symmetric case. The BCC morphology experiences the order−order transition to a HEX morphology upon subsequent cooling. The HEX morphology is then converted to a LAM morphology upon further cooling. However, the symmetric diblock copolymer undergoes a second-order transition from the disordered state to the LAM morphology. This second-order transition was later shown to exist only for diblock copolymers of infinite molecular weight. Fluctuation corrections by Fredrickson and Helfand to Leibler's mean-field RPA theory revealed that the disorder−order transition for diblock copolymers of finite molecular weight is of first order even for the symmetric ones, and a direct transition to the HEX or LAM structure is possible.[12]

Recently, it has been shown experimentally by Russell et al. that the diblock copolymers of deuterated polystyrene (PS) and several lower alkyl polymethacrylates exhibit a microphase separation upon heating, or in other words, the lower critical ordering transition (LCOT).[13−15] The diblock copolymer of deuterated PS and poly(vinyl methyl ether) (PVME), denoted as P(S-*b*-VME), also revealed a strong evidence of the same behavior.[16] The LCOT behavior, which is analogous to the lower critical solution temperature (LCST) behavior of the corresponding polymer blends, is considered to have the entropic origin of microphase separation. It is the difference in volume fluctuations between constituent polymers that drives self-association. This behavior has been interpreted in terms of compressible RPA formulated by several research groups. Freed and coworkers were the first to incorporate finite compressibility into the incompressible RPA by allowing for vacancy.[17−24] Yeung et al.[25] and then Bidkar and Sanchez[26] have also used vacancies as a pseudosolvent in the incompressible RPA by employing the lattice fluid model[27,28] for describing compressibility. Hino and Prausnitz employed their own off-lattice equation-of-

[†] A member of Hyperstructured Organic Materials Research Center at Seoul National University, Seoul 151-742, Korea.

10.1021/ma000640m CCC: $20.00
Published on Web 01/13/2001

state model[29,30] in an approach similar to that of Yeung et al.[31] A different compressible RPA theory was recently formulated by the present author without recourse to pseudosolvent technique.[32] An off-lattice equation-of-state model, developed by Cho and Sanchez,[33] was combined with the general compressible RPA formalism by Akcasu et al.[34,35] The common feature of compressible RPA, irrespective of derivation methodology, is to provide effective RPA interaction fields that take compressibility effects present in a realistic block copolymer system into account.[36]

In the compressible RPA analyses just mentioned,[17−26,31,32] the compressibility effects on scattering behavior and stability limits for selected polymer blends or diblock copolymers have mostly been discussed by examining the inverse susceptibility, i.e., the quadratic-order term in the Landau expansion. It is then the objective of our study to generalize the compressible RPA theory, introduced by the present author, to be cast into a Landau free energy of quartic order for various microstructures, yet to be characterized,[37] of a LCOT diblock copolymer. The analysis of the formulated Landau free energy reveals the nature of phase transition and the equilibrium condition of transitions between various microphases. However, it should be kept in mind that the present theory possesses certain limitations. Chains are assumed to be ideal, so that no chain stretching effect is considered. As a mean-field Landau analysis has been used, the theory ignores any concentration fluctuation effects and is applicable to weakly segregating systems. In addition, a single harmonic is used to describe the ordered structures only to discuss here the three classical morphologies. Corrections to the present theory with the inclusion of fluctuation effects and multiple harmonics may yield changes in the mean-field phase diagram with various other morphologies included.

For the P(S-*b*-VME) melt, chosen here as a model system, it is found that the transition from the disordered state to an ordered state is of first order in the entire region of composition. The phase diagram for the copolymer system is shown to possess aspects apparently different from that for a UCOT system. It is also of our interest to investigate the fluctuations of free volume. We intuitively expect that microphase separation in LCOT diblock copolymers induces the inhomogeneity of free volume. Excess free volume may be present in the more compressible component. The periodicity of free volume inhomogeneity should then be the same as that of microphase domains. It turns out that this expectation is indeed in accord with the present Landau analysis.

II. Landau Expansion of Free Energy

1. Landau Expansion of Free Energy for Compressible Diblock Copolymers. Phase-segregating compressible diblock copolymer melts can be probed by considering the average thermal fluctuations in the packing density field, or the order parameter ψ_i, for monomers of the ith component:

$$\psi_i(\vec{r}) \equiv \langle \delta\eta_i(\vec{r}) \rangle = \langle \eta_i(\vec{r}) - \eta_i \rangle \tag{1}$$

where η_i is the bulk-averaged packing density of i-monomers that implies the fraction of volume occupied by all the i-monomers. The $\eta_i(\vec{r})$ denotes the local packing density of such monomers at a position $\vec{r}$. The brackets in eq 1 imply the thermal average. The Landau expansion for the system free energy can then be written in a tensorial equation of order parameter ψ_i utilizing the summation convention as

$$F = F_0 + \frac{1}{\beta}\sum_{n=2}^{\infty}\frac{1}{n!}\int \mathrm{d}\vec{q}_1 \cdots \mathrm{d}\vec{q}_n \times \Gamma^{(n)}_{i_1 \cdots i_n}(\vec{q}_1, \cdots, \vec{q}_n)\psi_{i_1}(\vec{q}_1)\ldots\psi_{i_n}(\vec{q}_n) \tag{2}$$

where $\beta = 1/kT$ has its usual meaning. The F_0 implies the free energy of a system of interest in a disordered state. In eqs 1 and 2, all the subscripts i and i_a's take either 1 or 2. In the above equation, the Fourier component of ψ_i has been used for the convenience of subsequent manipulation of the free energy. It is well-known that the $\vec{q}_i$ in eq 2 denotes physically the scattering vector. The coefficient $\Gamma^{(n)}_{i_1 \cdots i_n}$ is commonly known as the nth-order vertex function.

We can now formally define an external potential field U_i, which is conjugate to ψ_i. Equation 2 can then be written in a tensorial expression in terms of U_i as

$$F = F_0 + \sum_{n=2}^{\infty}\frac{(-\beta)^{n-1}}{n!}\int \mathrm{d}\vec{q}_1 \cdots \mathrm{d}\vec{q}_n \times G^{(n)}_{i_1 \cdots i_n}(\vec{q}_1, \cdots \vec{q}_n)U_{i_1}(\vec{q}_1)\cdots U_{i_n}(\vec{q}_n) \tag{3}$$

where the coefficient $G^{(n)}_{i_1 \cdots i_n}$ is called the nth-order monomer density correlation (or response) function. Considering that U_i and ψ_i are conjugate to each other, eqs 2 and 3 are interchangeable by using the Legendre transform ($F(U_i) = F(\psi_i) + \int \mathrm{d}\vec{q} U_i\psi_i$). Therefore, it can be shown that the order parameter ψ_i is given by the functional derivative of eq 3 as

$$\psi_{i_1}(\vec{q}_1) = \sum_{n=2}^{\infty}\frac{(-\beta)^{n-1}}{(n-1)!}\int \mathrm{d}\vec{q}_2 \cdots \mathrm{d}\vec{q}_n \times G^{(n)}_{i_1 \cdots i_n}(\vec{q}_1, \vec{q}_2, \cdots, \vec{q}_n)U_{i_2}(\vec{q}_2)\cdots U_{i_n}(\vec{q}_n) \tag{4}$$

The vertex function $\Gamma^{(n)}_{i_1 \cdots i_n}$ can be related to the more familiar correlation functions $G^{(2)}$, $G^{(3)}$, ..., $G^{(n)}$. Putting eq 4 into eq 2 yields

$$\Gamma^{(2)}_{ij}(\vec{q}_1, -\vec{q}_1) = G^{(2)^{-1}}_{ij}(\vec{q}_1, -\vec{q}_1) \tag{5}$$

where the superscript -1 indicates the inverse as usual. The second-order correlation function $G^{(2)}_{ij}(\vec{q}_1, -\vec{q}_1)$ is often denoted as $S_{ij}(\vec{q}_1)$. The higher-order vertex functions are obtained as

$$\Gamma^{(3)}_{ijk}(\vec{q}_1, \vec{q}_2, \vec{q}_3) = -G^{(3)}_{lmn}(\vec{q}_1, \vec{q}_2, \vec{q}_3)\, G^{(2)^{-1}}_{li}(\vec{q}_1, -\vec{q}_1) \times G^{(2)^{-1}}_{mj}(\vec{q}_2, -\vec{q}_2)\, G^{(2)^{-1}}_{nk}(\vec{q}_3, -\vec{q}_3) \tag{6}$$

$$\begin{aligned}\Gamma^{(4)}_{abcd}(\vec{q}_1, \vec{q}_2, \vec{q}_3, \vec{q}_4) = {} & [\int \mathrm{d}\vec{q}\; G^{(2)^{-1}}_{ij}(\vec{q}, -\vec{q})\{G^{(3)}_{imn}(\vec{q}, \vec{q}_1, \vec{q}_2)\, G^{(3)}_{jop}(-\vec{q}, \vec{q}_3, \vec{q}_4) + \\ & G^{(3)}_{imo}(\vec{q}, \vec{q}_1, \vec{q}_3)\, G^{(3)}_{jnp}(-\vec{q}, \vec{q}_2, \vec{q}_4) + \\ & G^{(3)}_{imp}(\vec{q}, \vec{q}_1, \vec{q}_4)\, G^{(3)}_{jno}(-\vec{q}, \vec{q}_2, \vec{q}_3)\} - \\ & G^{(4)}_{mnop}(\vec{q}_1, \vec{q}_2, \vec{q}_3, \vec{q}_4)]G^{(2)^{-1}}_{ma}(\vec{q}_1, -\vec{q}_1) \times \\ & G^{(2)^{-1}}_{nb}(\vec{q}_2, -\vec{q}_2)\, G^{(2)^{-1}}_{oc}(\vec{q}_3, -\vec{q}_3)\, G^{(2)^{-1}}_{pd}(\vec{q}_4, -\vec{q}_4)\end{aligned} \tag{7}$$

Equations 5−7 just given are the generalization of eqs III-14 to III-16 in ref 4 in the case of multiple-order parameters. It should be remembered that all the $\Gamma^{(n)}$ and $G^{(n)}$ vanish unless $\sum_{i=1}^{n}\vec{q}_i = 0$.

2. Compressible RPA for Block Copolymers. Recently, the present author developed a compressible RPA theory[32] to calculate S_{ij} for the analysis of phase segregation in compressible polymer blends and block copolymers by combining Akcasu et al.'s general compressible RPA formalism[34,35] with the Cho−Sanchez (CS) off-lattice equation-of-state model.[33] Here, we present an extension of our compressible RPA theory to include higher-order correlation functions. The basic idea of the theory is the same as that of the incompressible RPA by Leibler.[4] In estimating the fluctuations ψ_i in eq 4, the correlation functions $G^{(n)}$ are supposed to be equal to those of noninteracting Gaussian copolymer chain system, denoted as $G^{(n)0}$. The external potential U_i is then replaced with U_i^{eff}, which is corrected as $U_i^{\text{eff}} = U_i + W_{ij}\psi_j$ to properly take the interaction effects into account by a proper interaction field W_{ij}. The W_{ij} substitutes for the simple Flory−Huggins χ to account for the desired compressibility effects so that it is formulated from the CS model in the next section. The resultant self-consistent-field equation is solved in an iterative technique to obtain correlation functions in eqs A5, A9, and A10. However, there is a distinct difference between our compressible RPA and its incompressible counterpart. In the former approach, there is no need for a Lagrange multiplier, which has been used in the latter approach to ensure the incompressibility constraint. Thus, the compressible RPA requires one more order parameter than the incompressible cousin. The correlation functions are then put into eqs 5−7 to yield the vertex functions as[38]

$$\Gamma_{ij}^{(2)} = S_{ij}^{-1} = S_{ij}^{0^{-1}} + \beta W_{ij} \tag{8}$$

$$\Gamma_{ijk}^{(3)}(\vec{q}_1,\vec{q}_2,\vec{q}_3) = -S_{pi}^{0^{-1}}(\vec{q}_1)\, G_{plm}^{(3)^0}(\vec{q}_1,\vec{q}_2,\vec{q}_3)\, S_{lj}^{0^{-1}}(\vec{q}_2)\, S_{mk}^{0^{-1}}(\vec{q}_3) \tag{9}$$

$$\begin{aligned}\Gamma_{abcd}^{(4)}(\vec{q}_1,\vec{q}_2,\vec{q}_3,\vec{q}_4) = {}& [\int \mathrm{d}\vec{q}\; S_{ko}^{0^{-1}}(\vec{q})\{G_{ijk}^{(3)^0}(\vec{q}_1,\vec{q}_2,\vec{q})\, G_{opr}^{(3)^0}(-\vec{q},\vec{q}_3,\vec{q}_4) + \\ & G_{ipk}^{(3)^0}(\vec{q}_1,\vec{q}_3,\vec{q})\, G_{ojr}^{(3)^0}(-\vec{q},\vec{q}_2,\vec{q}_4) + \\ & G_{irk}^{(3)^0}(\vec{q}_1,\vec{q}_4,\vec{q})\, G_{ojp}^{(3)^0}(-\vec{q},\vec{q}_2,\vec{q}_3)\} - \\ & G_{ijpr}^{(4)^0}(\vec{q}_1,\vec{q}_2,\vec{q}_3,\vec{q}_4)]S_{ia}^{0^{-1}}(\vec{q}_1)\, S_{jb}^{0^{-1}}(\vec{q}_2)\, S_{pc}^{0^{-1}}(\vec{q}_3)\, S_{rd}^{0^{-1}}(\vec{q}_4)\end{aligned} \tag{10}$$

It can be easily seen that $\Gamma^{(2)}$ is strongly dependent on the interaction field W_{ij}. The higher-order vertex functions, $\Gamma^{(3)}$ and $\Gamma^{(4)}$, are, however, only dependent on the Gaussian correlation functions. Therefore, those vertex functions are of entropic origin, just as in the incompressible RPA. The more detailed procedure for the derivation of eqs 8−10 is well documented in Appendix A.

The Gaussian correlation functions $G^{(n)0}$ can be given for our study by a slight modification of those in Appendices B and C of ref 4. Those correlation functions in ref 4 need to be multiplied by the overall packing density η that implies the fraction of volume occupied by all the copolymer chains. Some selected correlation functions are explicitly written in Appendix B to illustrate this modification.

3. CS Model and Interaction Field W_{ij}. The interaction field W_{ij}, as a replacement of the Flory−Huggins χ in the incompressible RPA, implies the apparent exchange energy, in which compressibility effects are included. The derivation of interaction field W_{ij} from the CS model has well been presented in our previous communication.[32] We will briefly mention here the CS model and the final expression for W_{ij}.

Let us begin with the system description. The system of interest consists of N chains of A−B diblock copolymers with r_1 monomers of A type and r_2 monomers of B type in a fixed volume. As was in our previous communication,[32] each copolymer chain is simplified to be the linear chain of tangent spheres or monomers, and monomers comprising both blocks are assumed to have the identical diameter σ. The volume fraction ϕ_1 of A monomers is then given by

$$\phi_1 = \frac{r_1}{r_1 + r_2} \tag{11}$$

The ϕ_2 (=1 − ϕ_1) then indicates the volume fraction of B monomers. The CS model gives the following analytical free energy F_0 for the corresponding blends of A homopolymers with r_1 monomers and B homopolymers with r_2 monomers at the same volume fraction ϕ_i:

$$\begin{aligned}\frac{\beta F_0}{rN} = {}& \sum \frac{\phi_i}{r_i} \ln \frac{6\eta\phi_i I_i \Lambda_i^{3r_i}}{\pi r_i \sigma^3 z_i e} + \\ & \left\{\frac{3}{2}\left[\frac{1}{(1-\eta)^2} - \left(1 - \frac{1}{r}\right)\frac{1}{1-\eta}\right] - \frac{1}{r}\left[\ln(1-\eta) + \frac{3}{2}\right]\right\} + \\ & \frac{1}{2} f_{\mathrm{p}} \beta \bar{\epsilon} \cdot u(\eta)\end{aligned} \tag{12}$$

where I_i implies the symmetry number of i-chains, and Λ_i means the thermal de Broglie wavelength of monomers on i-chains. The symbol z_i implies the conformational partition function of Gaussian i-chains, which can be left as an unspecified constant. The symbol e indicates the transcendental number of 2.718. The η denotes again the overall packing density. The first term of eq 12 represents the ideal free energy of the Gaussian blend system. The second term inside the brackets describes contribution to the free energy from the excluded volume effects, where r implies the average chain size of the blend system. The last term in eq 12 stands for the attractive interactions between nonbonded monomers, where $u(\eta)$ describes the packing density dependence of such interactions as

$$u(\eta) = [(\gamma/C)^{p/3}\eta^{p/3} - (\gamma/C)^2\eta^2] \tag{13}$$

The γ and C in eq 13 are simply $1/\sqrt{2}$ and $\pi/6$, respectively. The exponent p and the prefactor f_p associated with it are equal to 12 and 4, respectively, if the attractive interactions between monomers are described by the conventional Lennard-Jones potential. The parameter $\bar{\epsilon}$, which is defined as $\bar{\epsilon} = \sum_{ij}\phi_i\phi_j \cdot \bar{\epsilon}_{ij}$, describes the characteristic energy of the blend, where $\bar{\epsilon}_{ij}$ implies the potential depth of the attractive interactions between two monomers on i- and j-chains. Equation 13 is formulated from considering a mean-field energy of locally packed nonbonded monomers of nearest neighbors. The contributions to the free energy from

the excluded-volume effects and the attractive interactions comprise the nonideal free energy.

The W_{ij} at zero q is first formulated from the second-order derivatives of the nonideal free energy with respect to the packing densities η_i's by requiring the correct spinodal conditions for a given blend system. Considering the range of concentration and monomer density correlations, W_{ij} at finite q is approximated to W_{ij} at zero q in the q region for a typical small-angle radiation scattering.[26,32] The interaction field W_{ij} for polymer blends is then adopted for the corresponding block copolymers because block copolymers are equivalent to blends in a local view.[32]

The W_{ij} consists of the two terms L_{ij} and $\epsilon_{ij}^{\text{app}}$, where the former is given by the excluded-volume effects and the latter by the attractive interactions in the system

$$\beta W_{ij} = L_{ij}(\eta) - \beta\epsilon_{ij}^{\text{app}}(\eta) \tag{14}$$

where L_{ij} and $\epsilon_{ij}^{\text{app}}$ are mathematically given as

$$L_{ij}(\eta) = \frac{3}{2}\left[\frac{4}{(1-\eta)^3} + \frac{6\eta}{(1-\eta)^4} - \left(2 - \frac{1}{r_i} - \frac{1}{r_j}\right)\frac{1}{(1-\eta)^2} - \left(\eta - \frac{\eta}{r}\right)\frac{2}{(1-\eta)^3}\right] + \left(\frac{1}{r_i} + \frac{1}{r_j}\right)\frac{1}{1-\eta} + \frac{\eta}{r}\frac{1}{(1-\eta)^2} \tag{15}$$

and

$$-\beta\epsilon_{ij}^{\text{app}}(\eta) = \beta\bar{\epsilon}_{ij}f_p\frac{u(\eta)}{\eta} + \beta\left(\sum_k \eta_k\{\bar{\epsilon}_{ik} + \bar{\epsilon}_{jk}\}\right)f_p\frac{\partial}{\partial\eta}\left(\frac{u(\eta)}{\eta}\right) + \frac{1}{2}\beta\left(\sum_{kl}\eta_k\eta_l\bar{\epsilon}_{kl}\right)f_p\frac{\partial^2}{\partial\eta^2}\left(\frac{u(\eta)}{\eta}\right) \tag{16}$$

As can be seen from eqs 14−16, the interaction matrix W_{ij} is symmetric.

III. Landau Analysis for Classical Morphologies

1. Approximation to Order Parameters. To investigate disorder−order or order−order transitions in LCOT diblock copolymers, the Landau free energy given in eq 2 should be minimized with respect to the order parameters. This formidable task can be simplified by adopting the approximation method suggested by Leibler in his RPA theory.[4] We will generalize the method in an appropriate way for our analysis.

Considering the translational invariance in the disordered state of a LCOT system, the quadratic term in eq 2, denoted as βF_2, can then be rewritten as

$$\beta F_2 = \frac{1}{2}\int d\vec{q}\,[\Gamma_{11}^{(2)}(\vec{q},-\vec{q})\,\psi_1(\vec{q})\,\psi_1(-\vec{q}) + \Gamma_{12}^{(2)}(\vec{q},-\vec{q})\,\psi_1(\vec{q})\,\psi_2(-\vec{q}) + \Gamma_{21}^{(2)}(\vec{q},-\vec{q})\,\psi_2(\vec{q})\,\psi_1(-\vec{q}) + \Gamma_{22}^{(2)}(\vec{q},-\vec{q})\,\psi_2(\vec{q})\,\psi_2(-\vec{q})] \tag{17}$$

The order parameter $\psi_i(\vec{q})$ can be expressed in a polar form as

$$\psi_i(\pm\vec{q}) = |\psi_i(\vec{q})|e^{\pm i\varphi(i)} \tag{18}$$

where $\varphi(i)$ implies the phase angle of ψ_i associated with $\vec{q}$. Inserting eq 18 into eq 17 yields

$$\beta F_2 = \frac{1}{2}\int d\vec{q}\,[\Gamma_{11}^{(2)}(\vec{q},-\vec{q})|\psi_1(\vec{q})|^2 + \Gamma_{12}^{(2)}(\vec{q},-\vec{q})|\psi_1(\vec{q})||\psi_2(\vec{q})|e^{i[\varphi(1)-\varphi(2)]} + \Gamma_{21}^{(2)}(\vec{q},-\vec{q})|\psi_2(\vec{q})||\psi_1(\vec{q})|e^{i[\varphi(2)-\varphi(1)]} + \Gamma_{22}^{(2)}(\vec{q},-\vec{q})|\psi_2(\vec{q})|^2] \tag{19}$$

The equilibrium values of $|\psi_i(\vec{q})|$ and $\varphi(i)$ are to be determined by the minimization of the free energy with respect to them. It turns out that all the $\Gamma_{ij}^{(2)}$'s, or S_{ij}^{-1}'s, are positive, as can be seen in a later section. The minimization of eq 19 with respect to $\varphi(i)$'s thus gives the following condition

$$\varphi(1) - \varphi(2) = \pi \tag{20}$$

By using the symmetry of $\Gamma_{ij}^{(2)}$, eq 19 can then be simplified to

$$\beta F_2 = \frac{1}{2}\int d\vec{q}\,[\Gamma_{11}^{(2)}(\vec{q},-\vec{q})|\psi_1(\vec{q})|^2 - 2\Gamma_{12}^{(2)}(\vec{q},-\vec{q})|\psi_1(\vec{q})||\psi_2(\vec{q})| + \Gamma_{22}^{(2)}(\vec{q},-\vec{q})|\psi_2(\vec{q})|^2] \tag{21}$$

Meanwhile, a simple mathematical manipulation of eq 21 yields

$$\beta F_2 = \frac{1}{2}\int d\vec{q}\left[\Gamma_{11}^{(2)}\left(\left|\psi_1(\vec{q})\right| - \frac{\Gamma_{12}^{(2)}}{\Gamma_{11}^{(2)}}\left|\psi_2(\vec{q})\right|\right)^2 + \frac{1}{\Gamma_{11}^{(2)}}(\Gamma_{11}^{(2)}\Gamma_{22}^{(2)} - [\Gamma_{12}^{(2)}]^2)\left|\psi_2(\vec{q})\right|^2\right] \tag{22}$$

For the second term in the integrand of eq 22, it can be shown that

$$\Gamma_{11}^{(2)}\Gamma_{22}^{(2)} - [\Gamma_{12}^{(2)}]^2 = S_{11}^{-1}S_{22}^{-1} - (S_{12}^{-1})^2 = \det[S_{ij}^{-1}] \tag{23}$$

As was shown in our previous communication on the compressible RPA, the $\det[S_{ij}]$ near spinodals exhibits a diverging peak at a certain $|\vec{q}| = q^*$ that carries information on the microphase-separated domain sizes.[4,32] Its inverse, $\det[S_{ij}^{-1}]$, possesses a profound minimum at $|\vec{q}| = q^*$. Such minimum of $\det[S_{ij}^{-1}]$ is positive before reaching spinodals. The minimum keeps decreasing to change its sign at $|\vec{q}| = q^*$, as the diblock copolymer enters into the unstable region. It can then be understood that the most important contributions to βF_2 should be given by the integrand with $|\vec{q}| = q^*$. The integral in eq 21 is, therefore, approximated by the discrete summation as $\int d\vec{q} \rightarrow \sum_{\vec{q}\in\{\pm\vec{Q}_n\}}$, where n indicates the proper number of wave vectors $\vec{Q}_n$ with $|\vec{Q}_n| = q^*$ for a given microphase morphology. The amplitude of the order parameter fluctuations is now redefined in a more familiar form as $|\psi_i(\vec{q})| = (1/\sqrt{n})\psi_n(i)$.[4] Using the new amplitude converts eq 21 into its approximate form as

$$\beta F_2 = \Gamma_{11}^{(2)}\psi_n(1)^2 + \Gamma_{22}^{(2)}\psi_n(2)^2 - 2\Gamma_{12}^{(2)}\psi_n(1)\psi_n(2) \tag{24}$$

where all $\Gamma_{ij}^{(2)}$'s are evaluated at q^*. The βF_2 in eq 24 is positive before reaching spinodals because of positive $\Gamma_{ij}^{(2)}$'s and $\det[S_{ij}^{-1}]$. After passing through spinodals, βF_2 becomes negative in some region of $\psi_n(1)$ and $\psi_n(2)$.

Within the suggested approximation, the order parameter $\psi_i(\vec{r})$ in real space is given by the superposition of plane waves with the wavenumber q^*

$$\psi_i(\vec{r}) = \frac{1}{\sqrt{n}}\psi_n(i)\sum_{a=1}^{n}\{e^{-i[\vec{Q}_a\cdot\vec{r}-\varphi_a]} + \text{complex conjugate}\} \tag{25}$$

where φ_a is associated with $\vec{Q}_a$.

The first term in the integrand of eq 22 also suggests that the most important region of the order parameter amplitudes to minimize eq 21 or 24 is in the neighborhood of $\psi_n(1)/\psi_n(2) = \Gamma^{(2)}_{12}/\Gamma^{(2)}_{11}$ or $\Gamma^{(2)}_{22}/\Gamma^{(2)}_{21}$, with indices reversed. These two ratios, $\Gamma^{(2)}_{i2}/\Gamma^{(2)}_{i1}$, are very close and become identical at spinodal points.

2. Higher-Order Terms of Free Energy for Various Morphologies. The determination of the condition of phase equilibrium between various ordered microdomain structures requires the cubic and quartic terms of the Landau free energy in eq 2. Such higher-order terms with only the most important fluctuations included can be written as

$$\beta F_3 = \frac{1}{3!}\sum_{\vec{q}_i\in\{\pm\vec{Q}_a\}}\Gamma^{(3)}_{ijk}(\vec{q}_1,\vec{q}_2,\vec{q}_3)\,\psi_i(\vec{q}_1)\,\psi_j(\vec{q}_2)\,\psi_k(\vec{q}_3) \tag{26}$$

$$\beta F_4 = \frac{1}{4!}\sum_{\vec{q}_i\in\{\pm\vec{Q}_a\}}\Gamma^{(4)}_{ijkl}(\vec{q}_1,\vec{q}_2,\vec{q}_3,\vec{q}_4)\,\psi_i(\vec{q}_1)\,\psi_j(\vec{q}_2)\times \psi_k(\vec{q}_3)\,\psi_l(\vec{q}_4) \tag{27}$$

The higher-order terms given above vary according to morphologies of interest. In our present study, we only deal with the three classical morphologies such as the BCC, HEX, and LAM structures. The detailed analysis will be given in the following sections. The complex morphologies are beyond the scope of our present work. Further improvement of the theory with harmonic corrections allowed may yield the complex morphologies.

2.1. HEX Morphology. The HEX morphology is characterized by the following three ($n = 3$) reciprocal lattice vectors in the Fourier space, whose lengths are q^*:[4]

$$\vec{Q}_1 = q^*(1,0,0);\quad \vec{Q}_2 = q^*\left(-\frac{1}{2},\frac{\sqrt{3}}{2},0\right);\quad \vec{Q}_3 = q^*\left(-\frac{1}{2},-\frac{\sqrt{3}}{2},0\right) \tag{28}$$

The cubic term of the Landau free energy can then be given as

$$\beta F_3 = \frac{12}{3!}\frac{1}{(\sqrt{3})^3}\Gamma^{(3)}_{ijk}(1)e^{i[\varphi_1(i)+\varphi_2(j)+\varphi_3(k)]}\psi_n(i)\,\psi_n(j)\,\psi_n(k) \tag{29}$$

where $\varphi_a(i)$ implies the phase angle of ψ_i associated with $\vec{Q}_a$. The $\Gamma^{(3)}_{ijk}(1)$ is given from eq 9 as

$$\Gamma^{(3)}_{ijk}(1) = -S^{0\ -1}_{pi}(q^*)\,G^{(3)^0}_{plm}(1)\,S^{0^{-1}}_{lj}(q^*)\,S^{0^{-1}}_{mk}(q^*) \tag{30}$$

where $G^{(3)^0}(1)$ is evaluated only in the case that the three scattering vectors from $\vec{q}_1$ to $\vec{q}_3$ form an equilateral triangle. It turns out that the uncoupled vertex functions, $\Gamma^{(3)}_{111}$ and $\Gamma^{(3)}_{222}$, are negative. This result suggests that

$$\varphi_1(i) + \varphi_2(i) + \varphi_3(i) = 0 \tag{31}$$

in order to minimize the free energy, where i equals either 1 or 2. For the remaining coupled ones, the sum of phase angles equals $\pm 180°$ by eqs 20 and 31. In the case of $\Gamma^{(3)}_{112}$ as an example, we have

$$\varphi_1(1) + \varphi_2(1) + \varphi_3(2) = -\varphi_3(1) + \varphi_3(2) = -\pi \tag{32}$$

The quartic term of the Landau free energy can also be written as

$$\beta F_4 = \frac{1}{4!}\frac{18}{(\sqrt{3})^4}\{\Gamma^{(4)}_{ijkl}(0,0)e^{i[\varphi_a(i)-\varphi_a(j)+\varphi_a(k)-\varphi_a(l)]} + 4\Gamma^{(4)}_{ijkl}(0,1)e^{i[\varphi_b(i)-\varphi_b(j)+\varphi_c(k)-\varphi_c(l)]}\}\psi_n(i)\,\psi_n(j)\,\psi_n(k)\,\psi_n(l) \tag{33}$$

where $\Gamma^{(4)}_{ijkl}(h_1,h_2)$ is given by

$$\begin{aligned}\Gamma^{(4)}_{abcd}(h_1,h_2) = [&S^{0^{-1}}_{ko}(\sqrt{h_1}q^*)G^{(3)^0}_{ijk}(h_1)G^{(3)^0}_{opr}(h_1) + \\ &S^{0^{-1}}_{ko}(\sqrt{h_2}q^*)G^{(3)^0}_{ipk}(h_2)G^{(3)^0}_{ojr}(h_2) + \\ &S^{0^{-1}}_{ko}(\sqrt{4-h_1-h_2}q^*)G^{(3)^0}_{irk}(4-h_1-h_2)\times \\ &G^{(3)^0}_{ojp}(4-h_1-h_2) - G^{(4)^0}_{ijpr}(h_1,h_2)]S^{0^{-1}}_{ia}(q^*)\times \\ &S^{0^{-1}}_{jb}(q^*)\,S^{0^{-1}}_{pc}(q^*)\,S^{0^{-1}}_{rd}(q^*)\end{aligned} \tag{34}$$

The h_1 and h_2 for $\Gamma^{(4)}_{ijkl}$ and $G^{(4)^0}_{ijkl}$ define the relative angles between scattering vectors, where $|\vec{q}_1 + \vec{q}_2| = \sqrt{h_1}q^*$ and $|\vec{q}_1 + \vec{q}_4| = \sqrt{h_2}q^*$. The h for $G^{(3)^0}_{ijk}$ is given similarly by the relation that $|\vec{q}_1 + \vec{q}_2| = \sqrt{h}q^*$.[4] For the HEX morphology, we only need $\Gamma^{(4)}_{ijkl}(h_1,h_2)$ from (0,0) and (0,1) contributions. In all cases, the sums of phase angles in eq 33 are definitely determined by eq 20, as shown in Table 1.

2.2. BCC Morphology. The BCC morphology in real space corresponds to the face-centered-cubic (FCC) structure in the Fourier space. This structure is characterized by the following six ($n = 6$) reciprocal lattice vectors, whose lengths are again q^*:[4]

$$\begin{aligned}&\vec{Q}_1 = \frac{q^*}{\sqrt{2}}(1,1,0);\quad \vec{Q}_2 = \frac{q^*}{\sqrt{2}}(-1,1,0);\quad \vec{Q}_3 = \frac{q^*}{\sqrt{2}}(0,1,1);\\ &\vec{Q}_4 = \frac{q^*}{\sqrt{2}}(0,1,-1);\quad \vec{Q}_5 = \frac{q^*}{\sqrt{2}}(1,0,1);\\ &\vec{Q}_6 = \frac{q^*}{\sqrt{2}}(1,0,-1)\end{aligned} \tag{35}$$

The cubic term of the Landau free energy for the BCC morphology can then be written as

$$\beta F_3 = \frac{1}{3!}\frac{12}{(\sqrt{6})^3}\Gamma^{(3)}_{ijk}(1)\{e^{i[\varphi_1(i)-\varphi_3(j)-\varphi_6(k)]} + e^{i[\varphi_1(i)-\varphi_4(j)-\varphi_5(k)]} + e^{i[\varphi_2(i)-\varphi_4(j)+\varphi_6(k)]} + e^{i[\varphi_2(i)-\varphi_3(j)+\varphi_5(k)]}\}\psi_n(i)\,\psi_n(j)\,\psi_n(k) \tag{36}$$

Just as in the case of the HEX morphology, phase angles in eq 36 for 111 or 222 correlations should be summed to zero because of the negative $\Gamma^{(3)}_{111}$ or $\Gamma^{(3)}_{222}$.

Table 1. Sum of Phase Angles ($\Delta\varphi = \varphi_a(i) - \varphi_a(j) + \varphi_b(k) - \varphi_b(l)$) for βF_4 in Eq 33 for the HEX Morphology

	(h_1,h_2)			(h_1,h_2)	
ijkl	(0,0)	(0,1)	*ijkl*	(0,0)	(0,1)
1111	0	0	2111	$-\pi$	$-\pi$
1112	π	π	2112	0	0
1121	$-\pi$	$-\pi$	2121	-2π	-2π
1122	0	0	2122	$-\pi$	$-\pi$
1211	π	π	2211	0	0
1212	2π	2π	2212	π	π
1221	0	0	2221	$-\pi$	$-\pi$
1222	π	π	2222	0	0

[a] There are only one $\vec{Q}_a$ and two $\vec{Q}_a$'s required to describe (0,0) and (0,1) contributions to βF_4, respectively.

$$\varphi_1(i) - \varphi_3(i) - \varphi_6(i) = 0$$
$$\varphi_1(i) - \varphi_4(i) - \varphi_5(i) = 0$$
$$\varphi_2(i) - \varphi_4(i) + \varphi_6(i) = 0$$
$$\varphi_2(i) - \varphi_3(i) + \varphi_5(i) = 0 \qquad (37)$$

Phase angles for the coupled vertex functions are summed to $\pm 180°$, again as in the case of the HEX morphology. For example, it can be easily shown in the case of 112 correlation that

$$\varphi_1(1) - \varphi_3(1) - \varphi_6(2) = \varphi_6(1) - \varphi_6(2) = \pi$$
$$\varphi_1(1) - \varphi_4(1) - \varphi_5(2) = \varphi_5(1) - \varphi_5(2) = \pi$$
$$\varphi_2(1) - \varphi_4(1) + \varphi_6(2) = -\varphi_6(1) + \varphi_6(2) = -\pi$$
$$\varphi_2(1) - \varphi_3(1) + \varphi_5(2) = -\varphi_5(1) + \varphi_5(2) = -\pi \qquad (38)$$

The quartic term for the BCC morphology requires $\Gamma^{(4)}_{ijkl}(h_1,h_2)$ not only from (0,0) and (0,1) contributions but also from (0,2) and (1,2) contributions.

$$\beta F_4 = \frac{1}{4!}\frac{36}{(\sqrt{6})^4}\{\Gamma^{(4)}_{ijkl}(0,0)e^{i[\varphi_a(i)-\varphi_a(j)+\varphi_a(k)-\varphi_a(l)]} + 8\Gamma^{(4)}_{ijkl}(0,1)e^{i[\varphi_b(i)-\varphi_b(j)+\varphi_c(k)-\varphi_c(l)]} + 2\Gamma^{(4)}_{ijkl}(0,2)e^{i[\varphi_a(i)-\varphi_d(j)+\varphi_e(k)-\varphi_e(l)]} + 2\Gamma^{(4)}_{ijkl}(1,2)(e^{i[\varphi_1(i)+\varphi_2(j)-\varphi_3(k)-\varphi_4(l)]} + e^{i[\varphi_1(i)-\varphi_2(j)-\varphi_5(k)-\varphi_6(l)]})\}\psi_n(i)\,\psi_n(j)\,\psi_n(k)\,\psi_n(l) \qquad (39)$$

For the former three cases, phase angles in eq 39 are determined by eq 20. All these results are summarized in Table 2. However, for the last one, phase angles for some correlations can be summed to either 0° or $\pm 180°$, as seen in this table. In the case of 1112 correlation as an example, $\Delta\varphi = \varphi_1(1) + \varphi_2(1) - \varphi_3(1) - \varphi_4(2)$ is equal to either $[\varphi_1(1) - \varphi_3(1) - \varphi_6(i)] + [\varphi_2(1) - \varphi_4(2) + \varphi_6(i)]$ or $[\varphi_1(1) - \varphi_4(2) - \varphi_5(i)] + [\varphi_2(1) - \varphi_3(1) + \varphi_5(i)]$. Putting $i = 1$ or 2 into it yields $\Delta\varphi = \pi$ or 2π by eqs 37 and 38. The same argument can be given for the other case that $\Delta\varphi = \varphi_1(1) - \varphi_2(1) - \varphi_5(1) - \varphi_6(2)$. The minimization of the free energy should then be additionally considered. In such cases, the $\Gamma^{(4)}_{ijkl}(1,2)$ is replaced with $-|\Gamma^{(4)}_{ijkl}(1,2)|$ and the following exponentials with $+1$.

2.3. LAM Morphology. The LAM morphology has only one base vector ($n = 1$). Therefore, the cubic term of the Laudau free energy should vanish, and the quartic term is simply given as

Table 2. Sum of Phase Angles ($\Delta\varphi = \varphi_a(i) \pm \varphi_b(j) \pm \varphi_c(k) \pm \varphi_d(l)$) for βF_4 in Eq 39 for the BCC Morphology

	(h_1,h_2)			
ijkl	(0,0)	(0,1)	(0,2)	(1,2)
1111	0	0	0	0
1112	π	π	π	π or 2π
1121	$-\pi$	$-\pi$	$-\pi$	π or 2π
1122	0	0	0	2π
1211	π	π	π	π or 2π
1212	2π	2π	2π	π or 2π
1221	0	0	0	π or 2π
1222	π	π	π	π or 2π
2111	$-\pi$	$-\pi$	$-\pi$	π or 2π
2112	0	0	0	π or 2π
2121	-2π	-2π	-2π	π or 2π
2122	$-\pi$	$-\pi$	$-\pi$	π or 2π
2211	0	0	0	2π
2212	π	π	π	π or 2π
2221	$-\pi$	$-\pi$	$-\pi$	π or 2π
2222	0	0	0	0

[a] There are only one $\vec{Q}_a$ required for (0,0) contribution and two $\vec{Q}_a$'s required for (0,1) and (0,2) contributions to βF_4. In the case of the (0,1) contribution, two $\vec{Q}_a$'s form either 60° or 120° between them. In the other case of the (0,2) contribution, two $\vec{Q}_a$'s should be selected to form the right angle. However, there are four $\vec{Q}_a$'s necessary to describe the (1,2) contribution to βF_4, as they are clearly expressed in eq 39.

$$\beta F_4 = \frac{1}{4!}\frac{6}{(\sqrt{1})^4}\Gamma^{(4)}_{ijkl}(0,0)e^{i[\varphi_a(i)-\varphi_a(j)+\varphi_a(k)-\varphi_a(l)]} \times \psi_n(i)\,\psi_n(j)\,\psi_n(k)\,\psi_n(l) \qquad (40)$$

The sum of phase angles in eq 40 is definitely determined just as in the case of the HEX or BCC morphology.

3. Determination of Transition Conditions. The Landau free energy of quartic order can now be written as

$$\beta\delta F = \beta F - \beta F_0 = \beta F_2 + \beta F_3 + \beta F_4 \qquad (41)$$

where each term in eq 41 has already been introduced for various classical morphologies. The disorder−order transition temperature is first calculated by numerically finding the condition that the minimum of the free energy, βF_a, for a certain ordered structure overtakes βF_0 in the disordered state

$$\beta\delta F_a[T,\psi_n(1),\psi_n(2)] = 0 \qquad (42)$$

The order−order transition temperatures are then numerically calculated by finding the coexistence condition that

$$\beta\delta F_a[T,\psi^a_n(1),\psi^a_n(2)] = \beta\delta F_b[T,\psi^b_n(1),\psi^b_n(2)] \qquad (43)$$

where βF_a and βF_b are the minimum free energies for two selected *a* and *b* morphologies, respectively.

IV. Calculation of Phase Diagrams

In this section, we present the phase diagram of a diblock copolymer melt that exhibits LCOT behavior. The system chosen here is P(S-*b*-VME), which revealed a strong evidence of LCOT behavior by showing the increase of the scattering intensity with temperature.[16] This system is of our particular interest because the predicted microphase separation, driven by compressibility difference between PS and PVME, yields a spinodal line skewed toward the more compressible

PVME-rich side.[31,32] Therefore, a symmetric P(S-*b*-VME) melt loses its conventional position as the system providing the threshold of stability limits.

To calculate phase equilibrium condition of the P(S-*b*-VME) melt, various molecular parameters, σ_i, $\bar{\epsilon}_{ij}$, and r_i, are required. Hereafter, the subscripts 1 and 2 indicate PS and PVME, respectively. Following our previous work,[32] PS is characterized by $\sigma_1 = 4.04$ Å and $\bar{\epsilon}_{11}/k = 4107$ K. The characteristic parameters representing PVME are given by $\sigma_2 = 3.90$ Å and $\bar{\epsilon}_{22}/k = 3645$ K. The present theory deals only with the case that all the σ_i's are identical for simplification purposes. The discrepancy in monomer diameters for PS and PVME is resolved by employing the average monomer diameter, $\sigma = (\sigma_1 + \sigma_2)/2$, for both polymers. The theoretical chain sizes, r_1 and r_2, are obtained from the closed packed molecular volume V_i^*, which is defined as $\pi\sigma^3 r_i/6\mathrm{MW}_i$, where MW_i is the molecular weight of a constituent polymer. The V_i^*'s for PS and PVME are determined as 0.418 57 and 0.429 06 cm^3/g, respectively. The overall MW of P(S-*b*-VME), which is $\mathrm{MW}_1 + \mathrm{MW}_2$, is set to 1 000 000. If each MW_i is assigned to a certain value, then each block size r_i is determined. The cross-interaction parameter, $\bar{\epsilon}_{12}$, is estimated by $\bar{\epsilon}_{12} = 1.00264(\bar{\epsilon}_{11}\bar{\epsilon}_{22})^{1/2}$, which was obtained from the analysis of phase segregating deuterated PS/PVME blends.[32]

The overall packing density η of the system is determined by numerically solving the following equation of state from eq 12

$$\eta^2 \frac{\partial F_0}{\partial \eta} = r_T N v^* P \tag{44}$$

where r_T ($= r_1 + r_2$) is the overall chain size and v^* ($=\pi\sigma^3/6$) indicates the volume of a monomer in the system. The P implies the external pressure, which is fixed at the atmospheric pressure (0.1 MPa) in all the following calculations of microphase equilibria.

The present study is a generalization of Leibler's weak segregation limit theory[4] to LCOT diblock copolymers. In the approach by Leibler, the leading harmonic representation of the order parameter fluctuations with the largest growth rate was employed to analyze the formulated Landau free energy near spinodals. The fastest-growing fluctuations are those with the wavenumber q^*, at which det[S^{-1}] possesses a profound minimum. This situation is depicted in Figure 1, where det[S^{-1}] for the P(S-*b*-VME) melt is shown. In this figure, the volume fraction ϕ_1 of PS is set to 0.293. It should be noted that det[S^{-1}] is decreased upon heating; i.e., segregation is induced by heating. Unlike the behavior of det[S^{-1}], all the individual S_{ij}^{-1}'s are, however, well above zero and slowly varying, as can be seen in Table 3.

In characterizing thermally induced microphase separation in the LCOT diblock copolymer, one requires not only composition and temperature but also molecular parameters such as self ($\bar{\epsilon}_{ii}$) and cross-interaction ($\bar{\epsilon}_{ij}$) parameters and the sizes of polymers comprising the copolymer. These molecular parameters give a proper description of compressibility difference between constituent polymers, which is the driving force of microphase separation in the given system.

The dimensionless squared wavenumber, $x^* = q^{*2}R_G^2$, where R_G is the gyration radius of P(S-*b*-VME) chains, is plotted in Figure 2 as a function of ϕ_1. This common figure implies that the periodicity of ordered patterns is largest at $\phi_1 = 0.5$ and becomes smaller as ϕ_1 departs from 0.5.

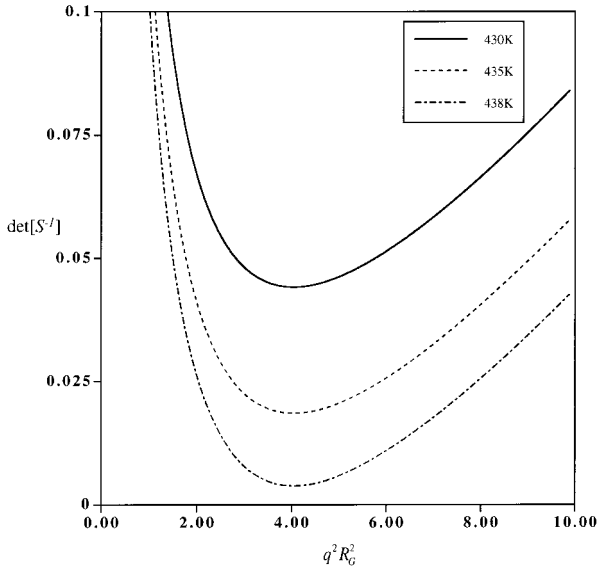

Figure 1. The det[S^{-1}] plotted as a function of squared dimensionless wave vector $q^2R_G^2$ for the P(S-*b*-VME) melt with MW of 1 000 000 at $\phi_1 = 0.293$ and at the indicated temperatures. The decrease of det[S^{-1}] is induced by heating, which implies the LCOT behavior of this system.

Table 3. Inverse Second-Order Correlation Functions, S_{ij}^{-1}'s, at $T = 438$ K and at $\phi_1 = 0.293$ in the Indicated Region of Squared Dimensionless Wave Vector $q^2R_G^2$

$q^2R_G^2$	S_{11}^{-1}	S_{12}^{-1}	S_{22}^{-1}
0.02	43.0767	44.1661	45.4759
1.00	42.9850	44.2041	45.4602
2.00	42.9841	44.2045	45.4601
3.00	42.9840	44.2046	45.4601
4.00	42.9840	44.2047	45.4601
5.00	42.9841	44.2047	45.4602
6.00	42.9842	44.2048	45.4603
7.00	42.9843	44.2048	45.4603
8.00	42.9845	44.2048	45.4604
9.00	42.9846	44.2048	45.4605

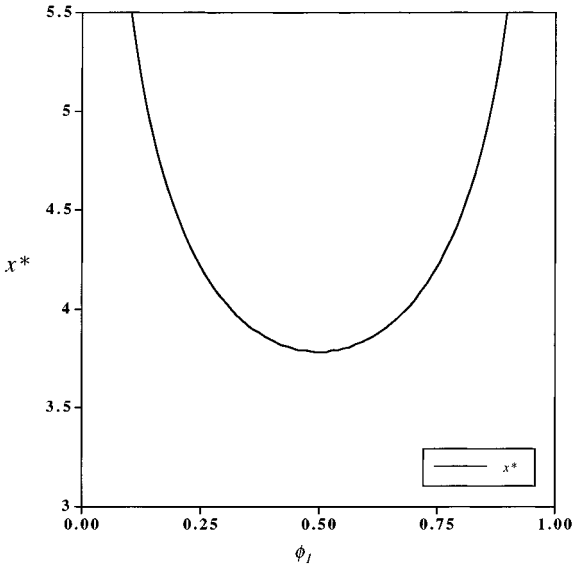

Figure 2. Dimensionless squared wavenumber x^* ($=q^{*2}R_G^2$) plotted as a function of ϕ_1.

The most distinct difference between the present analysis for LCOT systems and the incompressible RPA for UCOT systems lies in the vertex functions $\Gamma^{(n)}$'s as

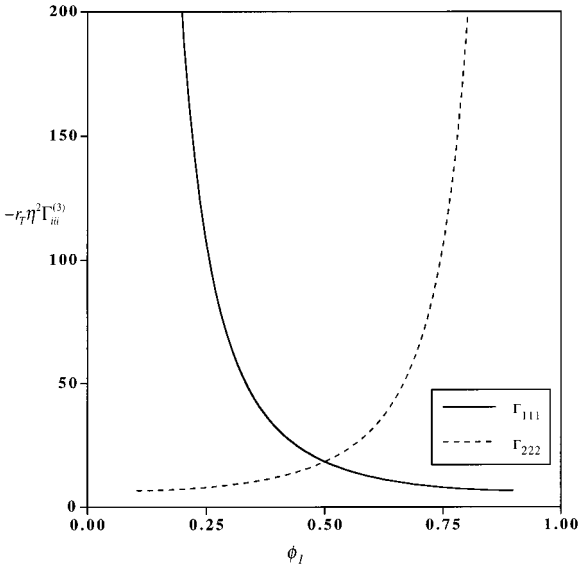

Figure 3. Combined third-order vertex function, $-r_T\eta^2\Gamma_{111}$ or $-r_T\eta^2\Gamma_{222}$, plotted as a function of ϕ_1.

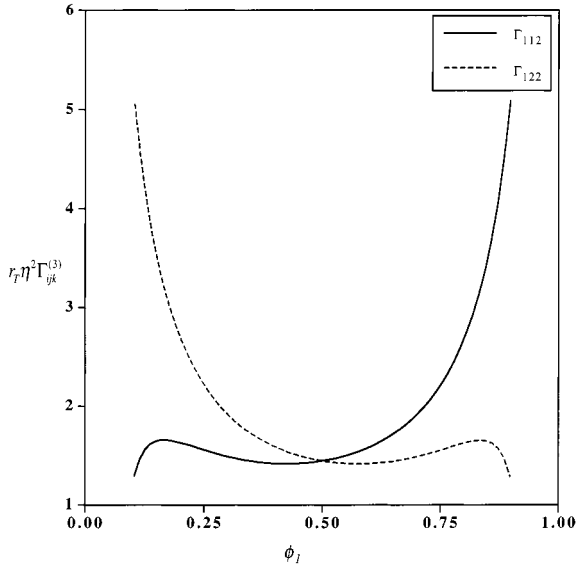

Figure 4. Coupled vertex function, $r_T\eta^2\Gamma_{112}$ or $r_T\eta^2\Gamma_{122}$, plotted as a function of ϕ_1.

in eqs 9 and 10. There are 2^n such vertex functions here in contrast to only one for the incompressible RPA.[4] Figure 3 shows the plot of $-r_T\eta^2\Gamma^{(3)}_{111}$ and $-r_T\eta^2\Gamma^{(3)}_{222}$ as a function of ϕ_1. These combined functions, which correspond to $-N\Gamma_3$ in Leibler's incompressible RPA,[4] are independent of the chain size and the system density. It is easily seen in this figure that these vertex functions are negative over the entire region of ϕ_1. It is also seen that $\Gamma^{(3)}_{111}$ or $\Gamma^{(3)}_{222}$ is nonvanishing even at $\phi_1 = 0.5$. It should be recalled that the vanishing Γ_3 at $\phi_1 = 0.5$ is characteristic of the incompressible approach. It is observed in Figure 3 that $-r_T\eta^2\Gamma^{(3)}_{222}$ can be given by reversing $-r_T\eta^2\Gamma^{(3)}_{111}$ around $\phi_1 = 0.5$. In Figure 4, the coupled third-order vertex functions, $r_T\eta^2\Gamma^{(3)}_{112}$ and $r_T\eta^2\Gamma^{(3)}_{122}$, are plotted against ϕ_1. They form again the reverse image to each other around $\phi_1 = 0.5$. While $\Gamma^{(3)}_{111}$ is negative, the coupled $\Gamma^{(3)}_{112}$ and $\Gamma^{(3)}_{122}$ become either positive or negative according to the composition. However, such coupled vertex functions are far less than the uncoupled $\Gamma^{(3)}_{111}$ or $\Gamma^{(3)}_{222}$ in the order of magnitude.

Table 4. $\eta^3\Gamma^{(4)}_{1111}$ for Various (h_1,h_2) Sets at the Indicated Compositions

	(h_1,h_2)			
ϕ_1	(0,0)	(0,1)	(0,2)	(1,2)
0.103	25028.10	25086.96	25096.07	25138.31
0.202	2025.98	2037.60	2039.94	2047.98
0.293	533.00	537.65	538.69	541.89
0.397	183.92	186.07	186.58	188.09
0.492	89.69	90.92	91.21	92.11
0.589	50.74	51.50	51.67	52.26
0.690	32.29	32.78	32.87	33.28
0.792	23.03	23.34	23.39	23.68
0.898	19.33	19.50	19.50	19.69

Table 5. $\eta^3\Gamma^{(4)}_{ijkl}(0,0)$ for Several Selected Correlations at the Indicated Compositions

ϕ_1	$\Gamma^{(4)}_{1112}$	$\Gamma^{(4)}_{1122}$	$\Gamma^{(4)}_{1212}$	$\Gamma^{(4)}_{1221}$
0.103	16.83	0.28	−525.81	502.18
0.202	3.56	−1.26	−162.29	148.28
0.293	1.00	−1.26	−97.08	86.34
0.397	−0.13	−1.18	−72.19	63.08
0.492	−0.70	−1.16	−66.12	57.44
0.589	−1.22	−1.18	−70.60	61.62
0.690	−1.91	−1.25	−90.59	80.26
0.792	−3.28	−1.27	−155.53	141.81
0.898	−7.86	0.32	−532.13	508.43

Other remaining vertex functions are identical to either $\Gamma^{(3)}_{112}$ or $\Gamma^{(3)}_{122}$. Figures 3 and 4 imply that $\Gamma^{(3)}_{111}$, or equivalently $\Gamma^{(3)}_{222}$, among the third-order vertex functions gives the most important contribution to βF_3.

The fourth-order vertex function $\Gamma^{(4)}_{ijkl}$ requires four scattering vectors from $\vec{q}_1$ to $\vec{q}_4$ to form suitable geometrical shapes in accord with a given microphase morphology. The shape made by four $\vec{q}_i$'s is characterized by the (h_1,h_2) set. For the classical morphologies, one needs to calculate $\Gamma^{(4)}_{ijkl}$ from (0,0), (0,1), (0,2), and (1,2) contributions. In Table 4, we tabulated $\eta^3\Gamma^{(4)}_{1111}$ for the four sets of (h_1,h_2) against ϕ_1. It is seen in this table that in general $\Gamma^{(4)}_{1111}(0,0) < \Gamma^{(4)}_{1111}(0,1) < \Gamma^{(4)}_{1111}(0,2) < \Gamma^{(4)}_{1111}(1,2)$, as was so for Γ_4 in Leibler's incompressible RPA analysis.[4] Table 5 shows $\eta^3\Gamma^{(4)}_{ijkl}(0,0)$'s representing several selected correlations at the indicated compositions. As seen in these two tables, the uncoupled $\Gamma^{(4)}_{1111}$ or $\Gamma^{(4)}_{2222}$ gives the most important contribution to βF_4.

Considering all the features of the formulated Landau free energy for a LCOT system, it can now be determined whether a given system is in a disordered state or in an ordered state (BCC, HEX, or LAM). Figure 5 shows all the calculated transition lines including the disorder−order and the order−order transitions for the P(S-*b*-VME) melt. The sequence of transitions is found to be the same as that in Leibler's incompressible RPA theory for UCOT systems: disorder → BCC → HEX → LAM.[4] However, there are number of aspects that differentiate the present analysis from Leibler's. It is seen in this figure that the spinodal line is entirely enclosed by the transition line from the disordered state to the metastable BCC mesophase. This result implies that the phase transition is of first order in the entire composition range. Even though the current approach is based on a mean-field analysis, the incorporation of finite compressibility in this LCOT system does not produce any second-order transition. In addition, there is a finite temperature range for the BCC or HEX morphology to be stable even at $\phi_1 = 0.5$. Such a peculiar phase diagram in Figure 5 for the LCOT system

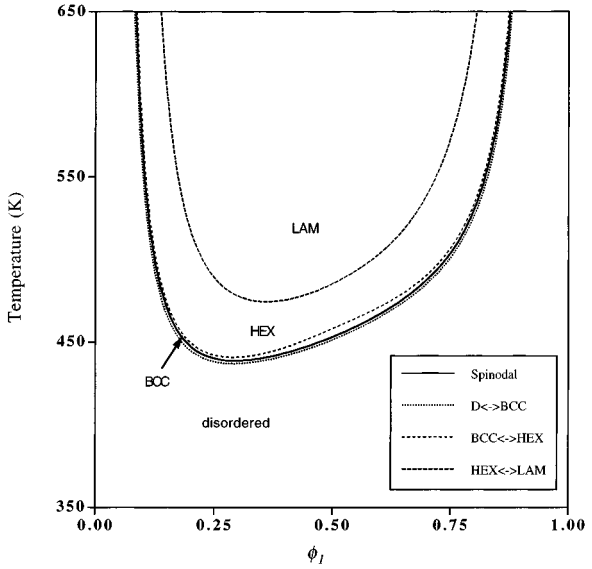

Figure 5. Phase diagram for the P(S-*b*-VME) melt with MW of 1 000 000. It should be noted that the transition line from a disordered state (D) to the metastable BCC mesophase entirely encloses the spinodal line. This figure suggests that phase transition for the copolymer is of first order in the whole range of ϕ_1. Further heating induces subsequent order−order transitions.

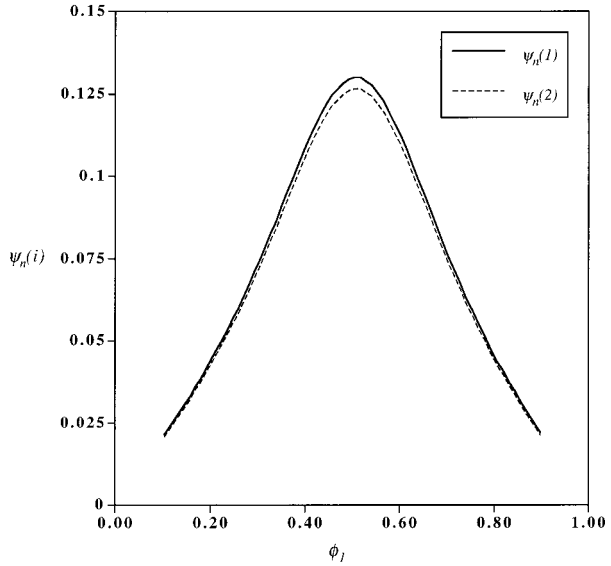

Figure 6. Amplitude parameter $\psi_n(i)$ for the packing density fluctuations at the disorder−order transition plotted as a function of ϕ_1. It is noted that $\psi_n(1)$ for PS is larger than $\psi_n(2)$ for PVME by ∼3% in the region of ϕ_1 in this figure.

originates in the nonvanishing and negative $\Gamma^{(3)}_{111}$ or $\Gamma^{(3)}_{222}$ in Figure 3.

In Figure 6, the amplitude $\psi_n(i)$ of the order parameter fluctuations for the constituent polymers is plotted against the composition in the case of the disorder → BCC transition. We first observe that $\psi_n(1)$ for PS is larger than $\psi_n(2)$ for PVME by ∼3% in the region of ϕ_1 in Figure 6. Such differences in $\psi_n(i)$'s are considered to reflect the fact that η of pure PS is larger than that of pure PVME at a given temperature; PS is less compressible than PVME. It is also observed that the amplitude $\psi_n(i)$ for the disorder−order transition possesses a maximum at $\phi_1 = 0.5$. This behavior can be illuminated by examining the packing densities η_1 and η_2 for each block at the transition temperatures. Smaller

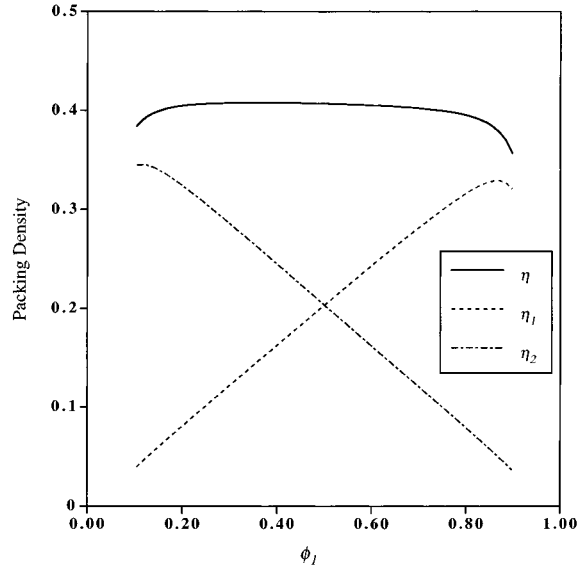

Figure 7. Packing densities at the disorder−order transition points as a function of ϕ_1.

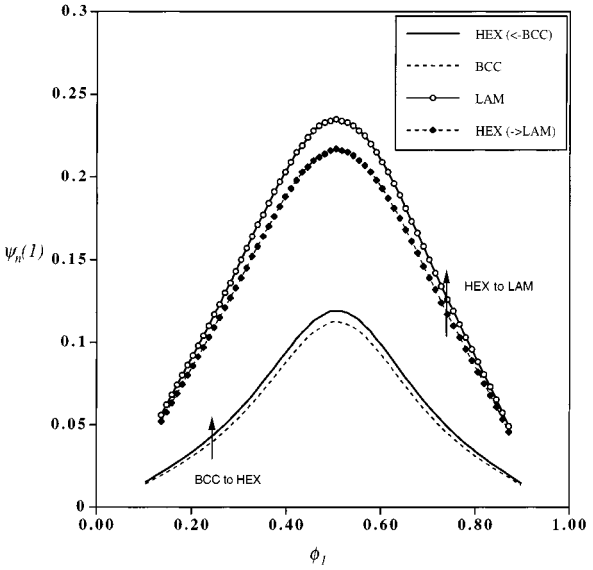

Figure 8. Amplitude parameter $\psi_n(1)$ for the packing density of PS plotted as a function of ϕ_1. The solid and dashed lines without symbols represent HEX and BCC morphologies, respectively, at the BCC → HEX transition. The open circle and the filled diamond indicate LAM and HEX morphologies, respectively, at the HEX → LAM transition.

η_i of the two should guide the maximum allowable packing density fluctuations. In Figure 7, we plot all the packing densities calculated at the transition points. As seen in this figure, the smaller η_i finds a maximum at $\phi_1 = 0.5$ and gradually decreases as one component becomes richer. This result then explains the composition dependence of $\psi_n(i)$ in Figure 6.

Figure 8 depicts the fluctuation amplitude $\psi_n(1)$ for PS at the BCC → HEX and the HEX → LAM transitions. The composition dependence of $\psi_n(1)$ for both cases is the same as in Figure 6. We observe that $\psi_n(1)$ of the BCC microphase at the BCC → HEX transition is slightly lowered from that at the disorder → BCC transition. The HEX → LAM transition requires much larger fluctuations in the order parameters than the BCC → HEX transition as the transition temperature at a given ϕ_1 is increased to a substantial extent. Such a leap in the transition temperatures shown in Figure

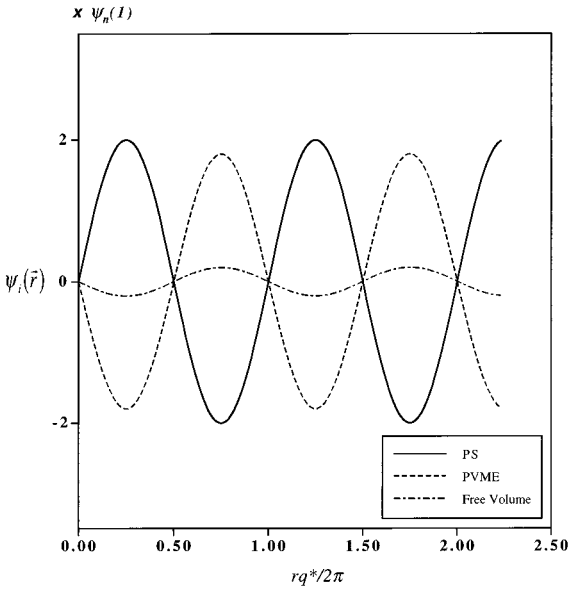

Figure 9. Schematic behavior of various order parameters, $\psi_i(\vec{r})$, for the LAM morphology in the direction perpendicular to lamellar layers. It should be noted that free volume fluctuates with the same wavenumber q^* as the packing densities of PS and PVME. It is also seen that the fluctuations of free volume are in phase with those of the packing density of the more compressible PVME.

5 suggests that the HEX → LAM transition can be more appropriately analyzed with a theory going beyond the weak segregation limit. If $\psi_1(\vec{r})$ for the LAM morphology in real space is probed in the direction perpendicular to lamellar layers, eq 25 yields in this case $\psi_1(\vec{r}) = 2\psi_n(1) \cos rq^*$. It is seen from Figure 8 that $\psi_n(1)$ at $\phi_1 = 0.5$ for the LAM morphology reads 0.235 at the HEX → LAM transition. Our calculation yields $\eta = 0.40$ at $\phi_1 = 0.5$ and at the corresponding transition temperature. The η_1 ($=\phi_1\eta$) for PS is then equal to 0.20. Therefore, there is some region of each microphase domain, in which either $\eta_1(\vec{r}) \geq \eta$ (PS only) or $\eta_1(\vec{r}) \leq 0$ (PVME only); i.e., one of the two components is completely excluded. The interface between two microphase domains is not sufficiently smooth.

As the P(S-*b*-VME) melt microphase separates, the distribution of free volume becomes inhomogeneous. The fluctuations of free volume fraction can be probed by considering the deviation of local free volume fraction $\eta_f(\vec{r})$ from its bulk average, which is given as $\langle\delta\eta_f(\vec{r})\rangle = -[\psi_1 + \psi_2]$. Along the direction perpendicular to the lamellar layers again, the $\psi_2(\vec{r})$ should fluctuate as $\psi_2(\vec{r}) = -2\psi_n(2) \cos rq^*$ because of the phase angle difference of 180°. The $\eta_f(\vec{r})$ can then be shown to fluctuate as $\langle\delta\eta_f(\vec{r})\rangle = -2[\psi_n(1) - \psi_n(2)] \cos rq^*$. This situation is schematically drawn in Figure 9. As $\psi_n(1) > \psi_n(2)$, the fluctuations of free volume fraction are in phase with those of the packing density for the more compressible PVME. This result is coincident with our intuitive expectation given in the Introduction. The fluctuation amplitude of free volume is, however, only ~3% of those of packing densities for the two blocks because $\psi_n(1)$ is again shown to be larger by ~3% than $\psi_n(2)$ at the HEX → LAM transition.

V. Concluding Remarks

We have investigated the phase behavior of P(S-*b*-VME), an LCOT diblock copolymer, with the help of the formulated Landau free energy of quartic order for various microphase structures. Finite compressibility, introduced into the Landau free energy through the effective interaction fields, gives the driving force of microphase separation in the copolymer. The relevant parameters to characterize phase equilibria discussed here are not only composition and temperature but also the self-interaction ($\bar{\epsilon}_{ii}$) and cross-interaction ($\bar{\epsilon}_{ij}$) parameters and the sizes of constituent polymers to properly describe compressibility difference between the two constituents. The present mean-field analysis gives the following aspects in the phase behavior of the copolymer that differ from those of typical UCOT diblock copolymers.

(1) A general sequence of microphase transition (disorder → BCC → HEX → LAM) upon heating is observed in the entire region of composition.

(2) Neither a critical point nor a second-order phase transition in the case of a symmetric copolymer is present because of the nonvanishing third-order vertex functions.

(3) The fluctuations of free volume are observed and shown to be in phase with those of the packing density of the more compressible component (PVME).

Even though only P(S-*b*-VME) is considered here, the aspects just mentioned should be common for any LCOT diblock copolymers.

All the features that this copolymer possesses are, in fact, based on one concept, which is the validity of one-wavenumber (q^*) approach for LCOT diblock copolymers. Our study reveals that such approach is indeed working. Free volume is selective: free volume favors a more compressible component. The fraction of free volume then fluctuates with the same wavenumber q^* as the local packing densities.

The incorporation of finite compressibility into UCOT diblock copolymers may also be useful in estimating the effect of pressure on the phase behavior of UCOT systems during processing. In this case, the driving force of microphase separation is the unfavorable energetics between constituent polymers. It is expected that excess free volume is present at the interface between microphase domains to screen such unfavorable interactions. Therefore, the analysis of UCOT systems necessitates the two-wavenumber approach because free volume fluctuates with the wavenumber $2q^*$ instead of q^* for the local packing density fluctuations. This topic may be visited in our forthcoming paper.

Acknowledgment. This work has been supported by Korea Science and Engineering Foundation through Hyperstructured Organic Materials Research Center.

Appendix A. RPA Equations for Compressible Systems

In this appendix, a detailed procedure for the extension of the compressible RPA by Cho[32] is presented. The basic concept is the same as that in Leibler's incompressible RPA.[4] The packing density fluctuations in eq 4 are assumed to be obtained from the correlation functions of noninteracting Gaussian copolymers and the corrected effective potentials. A simple way to solve such RPA equation is an iterative method as in Leibler's theory. The order parameter ψ_i is expressed as $\psi_i = \psi_i^{(1)} + \psi_i^{(2)} + \psi_i^{(3)}$, where each one corresponds to a separate contribution from the terms of different order in U_i. The first-order RPA equation is given as

$$\psi_i^{(1)} = -\beta S_{ij} U_j = -\beta S_{ij}^0 U_j^{\mathrm{eff}(1)} \quad \text{(A1)}$$

where the effective potential $U_j^{\mathrm{eff}(1)}$ in the compressible RPA is defined as

$$U_j^{\mathrm{eff}(1)} = U_j + W_{jk}\psi_k^{(1)} \quad \text{(A2)}$$

It should be noted that there is no Lagrange multiplier, which is used in Leibler's theory to ensure the incompressibility constraint. Equation A1 also yields

$$U_j^{\mathrm{eff}(1)} = S_{ij}^{0^{-1}} S_{ik} U_k \quad \text{(A3)}$$

The solution of eq A1 along with eq A2 is as follows:

$$\psi_i^{(1)} = -\{(\beta S_{ij}^0)^{-1} + W_{ij}\}^{-1} U_j \quad \text{(A4)}$$

Equation A4 yields the second-order correlation function S_{ij} as

$$\beta S_{ij} = \{(\beta S_{ij}^0)^{-1} + W_{ij}\}^{-1} \quad \text{(A5)}$$

The second- and third-order RPA equations are given as

$$\psi_i^{(2)}(\vec{q}) = \frac{1}{2}\beta^2 \int \mathrm{d}\vec{q}_2\, \mathrm{d}\vec{q}_3\, G_{ijk}^{(3)}(\vec{q},\vec{q}_2,\vec{q}_3)\, U_j(\vec{q}_2)\, U_k(\vec{q}_3) = -\beta S_{ij}^0 U_j^{\mathrm{eff}(2)} + \frac{1}{2}\beta^2 \int \mathrm{d}\vec{q}_2\, \mathrm{d}\vec{q}_3\, G_{ijk}^{(3)^0}(\vec{q},\vec{q}_2,\vec{q}_3) \times U_j^{\mathrm{eff}(1)}(\vec{q}_2)\, U_k^{\mathrm{eff}(1)}(\vec{q}_3) \quad \text{(A6)}$$

$$\psi_i^{(3)}(\vec{q}) = -\frac{1}{3!}\beta^3 \int \mathrm{d}\vec{q}_2\, \mathrm{d}\vec{q}_3\, \mathrm{d}\vec{q}_4\, G_{ijkl}^{(4)}(\vec{q},\vec{q}_2,\vec{q}_3,\vec{q}_4) \times U_j(\vec{q}_2)\, U_k(\vec{q}_3)\, U_l(\vec{q}_4) = -\beta S_{ij}^0 U_j^{\mathrm{eff}(3)} + \beta^2 \int \mathrm{d}\vec{q}_2\, \mathrm{d}\vec{q}_3\, G_{ijk}^{(3)^0}(\vec{q},\vec{q}_2,\vec{q}_3)\, U_j^{\mathrm{eff}(1)}(\vec{q}_2)\, U_k^{\mathrm{eff}(2)}(\vec{q}_3) - \frac{1}{3!}\beta^3 \int \mathrm{d}\vec{q}_2\, \mathrm{d}\vec{q}_3\, \mathrm{d}\vec{q}_4\, G_{ijkl}^{(4)^0}(\vec{q},\vec{q}_2,\vec{q}_3,\vec{q}_4)\, U_j^{\mathrm{eff}(1)}(\vec{q}_2) \times U_k^{\mathrm{eff}(1)}(\vec{q}_3)\, U_l^{\mathrm{eff}(1)}(\vec{q}_4) \quad \text{(A7)}$$

The corresponding effective potentials are defined as

$$U_j^{\mathrm{eff}(n)} = W_{jk}\psi_k^{(n)} \quad \text{(A8)}$$

where $n = 2$ and 3. There are also no Lagrange multipliers in eq A8. Solving the second- and third-order RPA equations in eqs A6 and A7 yields

$$G_{ijk}^{(3)}(\vec{q}_1,\vec{q}_2,\vec{q}_3) = C_{pi}(\vec{q}_1)\, G_{plm}^{(3)^0}(\vec{q}_1,\vec{q}_2,\vec{q}_3)\, C_{lj}(\vec{q}_2)\, C_{mk}(\vec{q}_3) \quad \text{(A9)}$$

$$G_{ijkl}^{(4)}(\vec{q}_1,\vec{q}_2,\vec{q}_3,\vec{q}_4) = C_{ai}(\vec{q}_1)\, G_{abcd}^{(4)^0}(\vec{q}_1,\vec{q}_2,\vec{q}_3,\vec{q}_4)\, C_{bj}(\vec{q}_2)\, C_{ck}(\vec{q}_3)\, C_{dl}(\vec{q}_4) - 3\int \mathrm{d}\vec{q}'\, \{C_{ai}(\vec{q}_1)\, G_{abc}^{(3)^0}(\vec{q}_1,\vec{q}_2,\vec{q}')\, C_{bj}(\vec{q}_2)[S_{cm}^{-1}(\vec{q}') - S_{cm}^{0^{-1}}(\vec{q}')]C_{dm}(\vec{q}')\, G_{def}^{(3)^0}(\vec{q}',\vec{q}_3,\vec{q}_4)\, C_{ek}(\vec{q}_3)\, C_{fl}(\vec{q}_4)\} \quad \text{(A10)}$$

where C_{jk} is defined by $S_{ij}^{0^{-1}} S_{ik}$. Equations A5, A9, and A10 are then put into eqs 5−7 to yield the desired eqs 8−10.

Appendix B. Gaussian Correlation Functions

The present RPA theory necessitates the Gaussian correlation functions, S_{ij}^0 and $G^{(n)^0}$, in analyzing a compressible diblock copolymer system with the overall packing density η. The second-order correlation function S_{ij}^0 can be written as

$$S_{11}^0(\vec{q}) = r_T \eta g_1(\phi_1,x)$$

$$S_{12}^0(\vec{q}) = \frac{r_T}{2}\eta[g_1(1,x) - g_1(\phi_1,x) - g_1(1-\phi_1,x)]$$

$$S_{22}^0(\vec{q}) = r_T \eta g_1(1-\phi_1,x) \quad \text{(B1)}$$

where x equals $q^2R_G^2$ as before and $g_1(\phi_1,x)$ denotes the modified Debye function defined as

$$g_1(\phi_1,x) = \frac{2}{x^2}[\phi_1 x + \mathrm{e}^{-\phi_1 x} - 1] \quad \text{(B2)}$$

The S_{ij}^0's in eq B1 for our study are obtained from those in Appendix B of ref 4. As seen in this equation, however, the η should be included in all the S_{ij}^0's. This modification is rationalized by the fact that the contact probabilities are diluted by the presence of free volume.

Higher-order correlation functions can also be given from those in Appendix C of ref 4. For example, the uncoupled correlation functions can be written as

$$G_{111}(h) = 2r_T^2\eta[2g_2(\phi_1,h) + g_2(\phi_1,1)] \quad \text{(B3)}$$

$$G_{1111}(h_1,h_2) = 8r_T^3\eta[f_1(\phi_1,h_1) + f_1(\phi_1,4-h_1-h_2) + f_1(\phi_1,h_2)] \quad \text{(B4)}$$

where the functions g_2 and f_1 are also given in Appendix C of ref 4. The modification of the correlation functions in ref 4 by η is clearly seen in eqs B3 and B4. All the remaining correlation functions of third and fourth order can be obtained from ref 4 in the same way.

References and Notes

(1) Aggarwal, S. L. *Block Copolymers*; Plenum Press: New York, 1970.
(2) *Developments in Block Copolymers-I*; Goodman, I., Ed.; Applied Science Publishers: New York, 1982.
(3) *Thermoplastic Elastomers*; Holden, G., Legge, N. R., Quirk, R. P., Schroeder, H. E., Eds.; Hanser: New York, 1996.
(4) Leibler, L. *Macromolecules* **1980**, *13*, 1602.
(5) Olvera de la Cruz, M. *Phys. Rev. Lett.* **1991**, *67*, 85.
(6) Olvera de la Cruz, M.; Mayes, A. M.; Swift, B. W. *Macromolecules* **1992**, *25*, 944.
(7) Milner, S. T.; Olmsted, P. D. *J. Phys. II* **1997**, *7*, 249.
(8) Hamley, I. W.; Bates, F. *J. Chem. Phys.* **1994**, *100*, 6813.
(9) Podneks, V. E.; Hamley, I. W. *JETP Lett.* **1996**, *64*, 617.
(10) Podneks, V. E.; Hamley, I. W. *Pis'ma Zh. Eksp. Teor. Fiz.* **1996**, *64*, 564.
(11) Hamley, I. W.; Podneks, V. E. *Macromolecules* **1997**, *30*, 3701.
(12) Fredrickson, G. H.; Helfand, E. *J. Chem. Phys.* **1987**, *87*, 697.
(13) Russell, T. P.; Karis, T. E.; Gallot, Y.; Mayes, A. M. *Nature* **1994**, *368*, 729.
(14) Karis, T. E.; Russell, T. P.; Gallot, Y.; Mayes, A. M. *Macromolecules* **1995**, *28*, 1129.
(15) Ruzette, A.-V. G.; Banerjee, P.; Mayes, A. M.; Pollard, M.; Russell, T. P.; Jerome, R.; Slawecki, T.; Hjelm, R.; Thiyagarajan, P. *Macromolecules* **1998**, *31*, 8509.
(16) Hashimoto, T.; Hasegawa, H.; Hashimoto, T.; Katayama, H.; Kamogaito, M.; Sawamoto, M.; Imai, M. *Macromolecules* **1997**, *30*, 6819.
(17) McMullen, W. E.; Freed, K. F. *Macromolecules* **1990**, *23*, 255.
(18) Dudowicz, J.; Freed, K. F. *Macromolecules* **1990**, *23*, 1519.
(19) Tang, H.; Freed, K. F. *Macromolecules* **1991**, *24*, 958.
(20) Tang, H.; Freed, K. F. *J. Chem. Phys.* **1991**, *94*, 1572.
(21) Dudowicz, J.; Freed, K. F. *J. Chem. Phys.* **1992**, *96*, 9147.
(22) Freed, K. F.; Dudowicz, J. *J. Chem. Phys.* **1992**, *97*, 2105.
(23) Dudowicz, J.; Freed, K. F. *Macromolecules* **1993**, *26*, 213.

(24) Dudowicz, J.; Freed, K. F. *J. Chem. Phys.* **1994**, *100*, 4653.
(25) Yeung, C.; Desai, R. C.; Shi, A. C.; Noolandi, J. *Phys. Rev. Lett.* **1994**, *72*, 1834.
(26) Bidkar, U. R.; Sanchez, I. C. *Macromolecules* **1995**, *28*, 3963.
(27) Lacombe, R. H.; Sanchez, I. C. *J. Phys. Chem.* **1976**, *80*, 2568.
(28) Sanchez, I. C.; Lacombe, R. H. *Macromolecules* **1978**, *11*, 1145.
(29) Song, Y.; Lambert, S. M.; Prausnitz, J. M. *Chem. Eng. Sci.* **1994**, *49*, 2765.
(30) Hino, T.; Prausnitz, J. M. *Fluid Phase Equilib.* **1997**, *138*, 105.
(31) Hino, T.; Prausnitz, J. M. *Macromolecules* **1998**, *31*, 2636.
(32) Cho, J. *Macromolecules* **2000**, *33*, 2228.
(33) Cho, J.; Sanchez, I. C. *Macromolecules* **1998**, *31*, 6650.
(34) Akcasu, A. Z.; Tombakoglu, M. *Macromolecules* **1990**, *23*, 607.
(35) Akcasu, A. Z.; Klein, R.; Hammouda, B. *Macromolecules* **1993**, *22*, 1238.
(36) In most of the compressible RPA theories for block copolymers,[25,31,32] LCOT behavior has been interpreted solely in terms of finite compressibility. Meanwhile, Freed and coworkers have taken into consideration in some of their works the effects of detailed monomer molecular structures on interaction fields in addition to compressibility effects.[22−24] In the very recent communication, it was argued by them that such specific interactions from the structural differences cause LCOT behavior in the diblock copolymers of PS and some poly(*n*-alkyl methacrylates) in the high pressure and high molecular weight limit. See: Dudowicz, J.; Freed, K. F. *Macromolecules* **2000**, *33*, 5292.
(37) Microphase morphologies to form upon heating and transitions between them for the P(S-*b*-VME) melt and other LCOT systems have not been characterized yet. In regard to this problem, one may find the experiments by Russell and coworkers on the thin films of a near symmetric poly(styrene-*b*-*n*-butyl methacrylate) melt, spin-coated onto a substrate surface. The interplay of surface-induced ordering and microphase separation to yield lamellar structures is observed in this case. See: Mansky, P.; Tsui, O. K. C.; Russell, T. P.; Gallot, Y. *Macromolecules* **1999**, *32*, 4832.
(38) Equations 8−10 are identical with eqs A9−A11 in the RPA study of block copolymer solutions by Fredrickson and Leibler, if the overall volume fraction of copolymers is replaced with η. See: Fredrickson, G. H.; Leibler, L. *Macromolecules* **1989**, *22*, 1238.

MA000640M